Numerical analysis of 3D printed joint of wooden structures regarding mechanical and fatigue behaviour

Petr Lehner, Přemysl Pařenica, David Juračka, Martin Krejsa
VSB – Technical University of Ostrava, Faculty of Civil Engineering, Department of Structural Mechanics, Czech Republic
petr.lehner@vsb.cz, http://orcid.org/0000-0002-1478-5027
premysl.parenica@vsb.cz, http://orcid.org/0000-0002-5491-1542
david.juracka@vsb.cz, https://orcid.org/0000-0001-8252-6433
martin.krejsa@vsb.cz, https://orcid.org/0000-0003-0571-2616

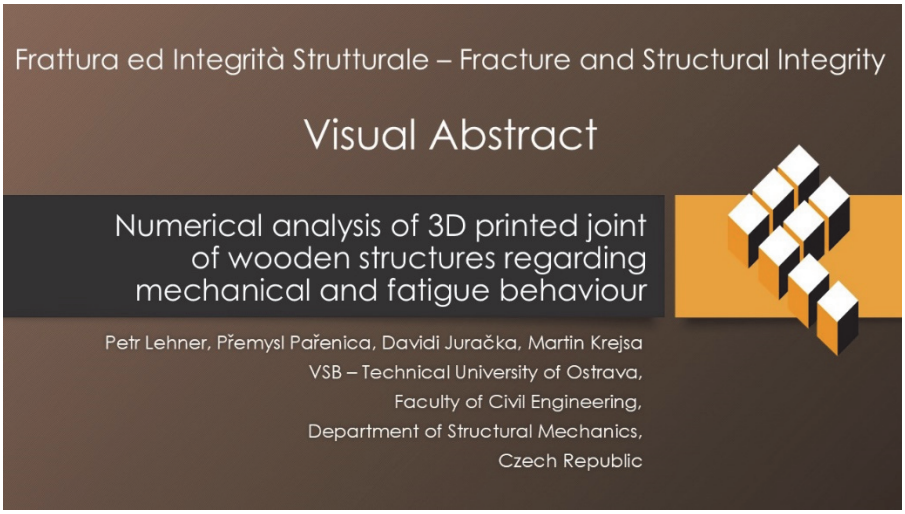

Citation: Lehner, P., Pařenica, P., Juračka, D., Krejsa, M., Numerical analysis of 3D printed joint of wooden structures regarding mechanical and fatigue behaviour, Fracture and Structural Integrity, 71 (2025) 151-163.

Received: 02.10.2024
Accepted: 16.10.2024
Published: 18.10.2024
Issue: 01.2025

KEYWORDS. 3D print, Polycarbonate, Wood, Numerical model, Fatigue.

INTRODUCTION

In recent years, 3D printing technology has increasingly come to the forefront of industrial and building design, which has also been reinforced by a growing interest in greener and more efficient design practices [17,23]. Considering global trends in sustainability and materials recycling, 3D printing is becoming an innovative method that not only enables cost-effective production of structural components but also provides flexibility in the design and optimization of building elements [10,24]. The increased number of applications brings with it the discovery of new problems and challenges. An example is the susceptibility of 3D printed features to failure due to brittleness or poorly chosen geometry detail. While 3D printing of concrete (composites) has gained considerable attention in past years and application success [9,19], an interesting and less explored area is the use of 3D printing of plastics and metals to produce fasteners for wooden structures. Wood, as a traditional and environmentally friendly building material, has in recent years started to regain the attention of architects and engineers, mainly due to its positive properties such as its lightweight, good insulating capacity and ability to store carbon [8,25]. However, joining timber elements remains technically challenging as traditional methods may not be suitable

from a sustainability perspective. Variable geometry, variety of shapes and a balance between cost and high aesthetic quality are also important. This is where the evaluation of the use of 3D printing comes in.

Aim of the research

This paper focuses on the possibilities of numerical modelling of 3D printed joints (see Fig. 1) of wooden structural elements, which has the potential to significantly push the boundaries of standard design methods. The goal of the research was not only to create accurate material models for 3D printed components but also to effectively analyze the interaction between the joint material and the structural wood. To achieve this goal, modern numerical methods based on the finite element method (FEM [6]) were used. The structure of the article is divided into several interrelated chapters. The first part is devoted to the theoretical background and sources of information for the preparation of models. The next section describes several variants of the models in terms of geometry, several variants of boundary conditions and a description of the parameters of the materials used. This is followed by a chapter with the results of the numerical analysis and a final summary. This approach allows a robust basis for comparison between numerical predictions and experimental results in the future.

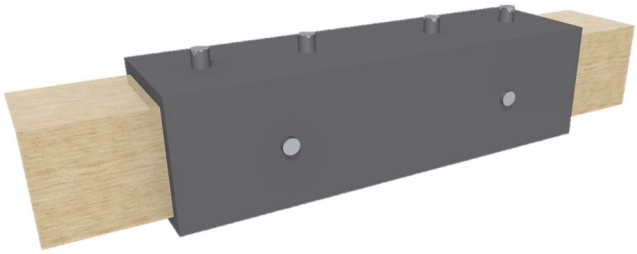

Figure 1: Visualization of the first variant of a 3D printed joint with connected wooden elements.

THEORETICAL AND EXPERIMENTAL BACKGROUND

3D printing in structural engineering

3D printing is an innovative additive manufacturing method that brings new possibilities to structural engineering by enabling the efficient and precise production of complex geometric shapes. On the other hand, its disadvantages include fragility and susceptibility to fracture problems [17,22], as well as instability of the material properties of the resulting products. Several 3D printing methods differ in the materials and processes used, such as FDM (fused deposition modelling), SLA (stereolithography) or SLS (selective laser sintering) [23]. Each of these methods has its advantages and disadvantages in terms of accuracy, speed, cost and characteristics of the final product. Plastics, composites, but also biopolymers are increasingly used in structural engineering, opening new possibilities for greener production. Recently, there has also been an increasing interest in recycled materials and wood as a building material, which is a step towards sustainability in construction projects [24].

Mechanics of timber frame structures

Timber frame structures have specific mechanical properties that must be considered when designing joints. Key principles include the behaviour of timber in bending, compression and torsion. Timber frame joints respond to different types of loads and environmental factors, which can affect their strength and deformation behaviour [16,18]. Mechanical elements such as nails, screws or bolts are often used in the design of timber joints. The effectiveness of these joints depends on many factors, including wood type, variations in thickness, angles and loads, and therefore a thorough knowledge of wood physics is essential for successful analysis and design [11,13].

Fatigue behavior 3D printed samples

Because 3D printed materials exhibit different mechanical properties compared to conventionally processed materials, it is important to investigate also their fatigue life. Microstructure caused by the printing technology, layer orientation, and possible defects were identified as the main factors affecting fatigue behaviour [5]. It is the layer orientation and the printing speed that significantly affect both the maximum durability and the number of cycles before failure [15]. Further research has shown that various intricate textures in critical detail areas of the samples can dramatically increase durability [5]. These studies show that a thorough understanding of fatigue behaviour and optimization of printing parameters are essential to ensure the reliability of 3D printed joints.

Experiments and previous research

The presented results are a preparation for future verification by experiments. Therefore, the loading schemes are based on two tests: tensile test according to ASTM D638-14 [2] and three-point bending of wood according to ASTM D 143-94 [1] and three-point bending of plastic according to ASTM D790 [4]. These standards were used as a template to develop boundary conditions for the numerical models. Tensile tests are used to measure mechanical properties of materials such as tensile strength, yield strength, and ductility. Three-point bending is then used to determine flexural modulus, yield strain, and fracture parameters. Experience was also drawn from previous experiments analyzing the interaction of wooden elements and 3D printed reinforcement [7]. Another source of information for the presented models was the extensive research on modelling wooden elements [12].

MODELLING OF JOINT

ANSYS 2024 R2 [3] software was used for FEM-based numerical analysis. The geometry (see below) was prepared based on the 3D printing limitations of the printer used (MK3+ from Prusa Research [20]) so that the models fully correspond to reality. The material properties and boundary conditions for the model are listed below. Since all variants were prepared as axisymmetric, a half model was possible and adequate results were obtained. One model includes approximately 41,000 nodes and 26,000 elements.

Geometry of variations

Two variants of the geometry with a different interaction of the wooden and 3D printed elements were analyzed. Fig. 2 shows the first (01) geometric variant and second (02) geometric variant of the analyzed connection. The setup consists of a printed joint into which two joined wooden elements are inserted. The first solution is the use of steel pins, and the second solution is the use of sliding stops (steel grade 8.8 is considered).

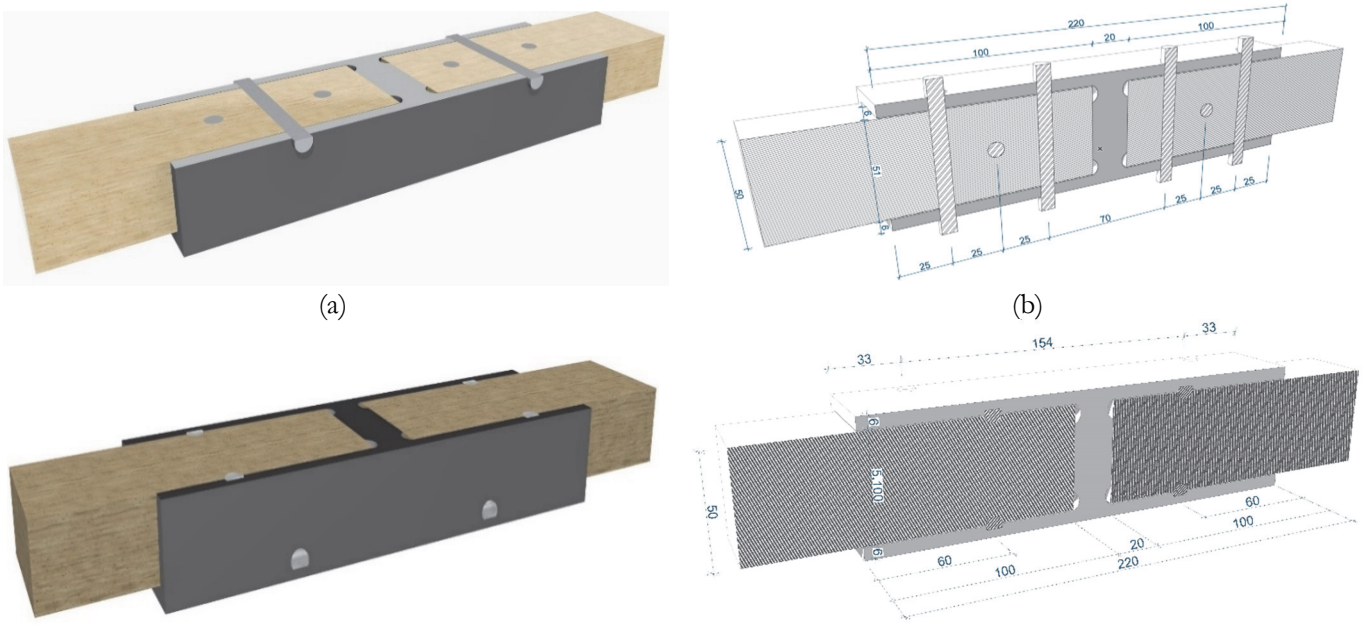

Figure 2: First (01) geometric variant of the 3D printed joint: (a) horizontal longitudinal cross-section, (b) dimensions [mm]. Second (02) geometric variant of the 3D printed joint: (c) horizontal longitudinal cross-section, (d) dimensions [mm].

Fig. 3 shows the prepared numerical (symmetric half longitudinally) model for both variants. The first variant of the geometry was prepared with the aim of making 3D printing as simple as possible and with the assumption of breaking in the wood part - splitting. The second variant has a more complex geometry based on the assumption of a better transfer of shear forces, which could lead to a more even load distribution on all materials.

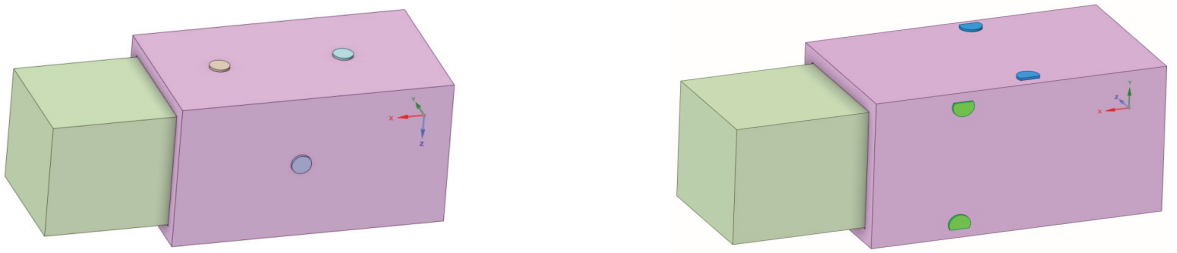

(a) (b)

Figure 3: Numerical model of: (a) first geometric variant (No. 01) and (b) second geometric variant (No. 02).

Materials parameters

The material properties required for the numerical model were in the first stage taken from the technical data sheets of the manufacturer of the printed material or literature sources. The 3D printed element is modelled and will be made from PC Blend (polycarbonate) [20], which is a polycarbonate filament designed for demanding applications. As this is an analysis of the joint behaviour of the joint and the material to be joined, it was also necessary to introduce the properties of wooden prisms, in this case of 50 x 50 mm cross-section, wood grade C24. As the element to be joined is inserted into the 3D printed joint in the case studied, it was necessary to use shear stops, which were considered from steel grade 8.8. The basic mechanical properties of all the materials used are given in Tab. 1. It should be noted that there is a weakness in the above numerical analysis, as the PC blend itself needs to be analyzed more in terms of its properties in different directions. This simplification is adopted due to the objectives of analyzing the critical points of the given design of the two variants.

Parameter	PC blend	Wood grade C24 [12]			Steel grade 8.8. [14]
		X	Y	Z	
Density [kg.m^3]	1220		380		7850
Modulus of elasticity [GPa]	1.90	9.20	0.74	0.40	210.000
Poisson ratio [-]	0.35	0.47	0.25	0.37	0.30
Tensile strength [MPa]	63	32	1	1	640

Table 1: Material properties for the numerical model.

Boundary conditions

All numerical models are prepared as half of the real sample (see Fig. 3). The contact surfaces between the materials are set to transfer only pressure and friction. Between wood and PC blend the friction coefficient is set to 0.25, between wood and steel pins the friction coefficient is set to 0.35, and between PC blend and steel pins, the friction coefficient is set to 0.25. The finite element mesh is set to an average element size of 8 mm, but smaller mesh elements are applied around the holes and critical points. Several load schemes were applied. The first was an axial tensile load. The sample load was applied using remote displacement from 0 to 8 mm in axial X. The second scheme was a simulation of a three-point bending in the direction of the Z-axis. The displacement from 0 to 20 mm was used. The third scheme was a three-point bending simulation in the Y-axis direction. The displacement from 0 to 20 mm was used too. For these three loading schemes, the response (force) results under load were obtained and these values were plotted along with the displacement in graphs. For the second and third schemes, the obtained forces are multiplied by 2 to give the result for the whole element. The force-displacement diagrams show the limit points, which correspond to the limit states for each material in the model. For wood, this is a shear stress value of 3 MPa [12], for PC blend it is an equivalent plastic strain value of 5% [20], and for steel, it is a yield stress value of 640 MPa [15]. The last, fourth, loading scheme is significantly different from the previous ones because it is related to fatigue parameters. In principle, the aim here is to evaluate the critical fatigue points on the 3D printed sample. The loading force is determined from the first loading scheme and the resulting maximum stresses. It should be noted, that the magnitude of the stresses does not play a role in this analysis. Cyclic loading is then applied to estimate the life durability. The critical stresses on the elements are confronted with the S-N curve for polycarbonate [21]. From the obtained value of the number of cycles, it is possible to determine the critical locations and which variant of the geometry has better resistance.

RESULTS

The objective of the numerical analysis was to evaluate the differences between two geometric variants of a 3D printed joint subjected to several different types of loading. Thus, the results are divided according to the types of models in terms of loading and boundary conditions.

First load scheme: axial tensile test

The first set of results are force-displacement diagrams obtained from two numerical models of axial tensile loads for both geometric variants (see Fig. 4). The limiting values for each material are highlighted and described in the diagrams. These milestones help to understand the progress of the load test and allow a direct comparison between the two geometric variants. Variant 02 performed more force with the same deformation than variant 01. The wood was the first to reach the limit in both variants. Steel showed the highest resistance. Interestingly, the limit value of the PC blend in variant 02 is higher than in variant 01. Figs. 5 to 7 shows the visualization of the individual limit values of the separate components (by material). It is possible to identify the critical details of each part.

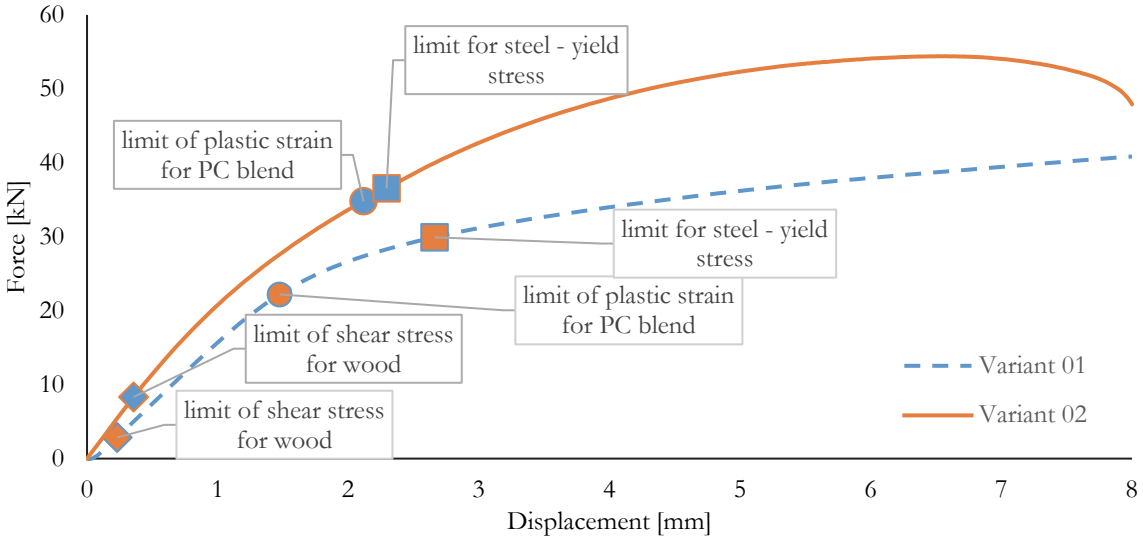

Figure 4: Force-displacement diagram for first load scheme (axial tensile test) for variants 01 and 02 with critical points for each material.

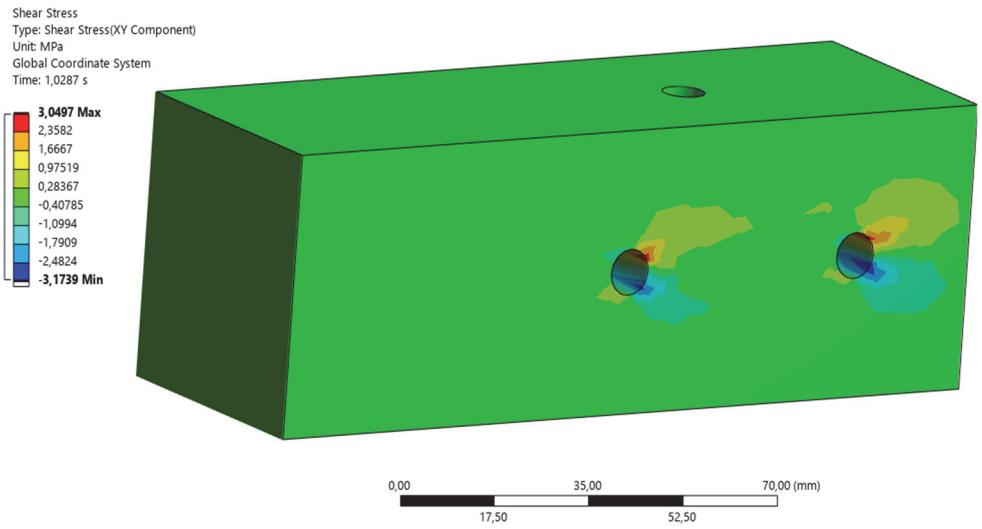

Figure 5: Visualization of results for limit milestones in the first loading scheme (axial tensile test): shear stress of timber variant No. 01.

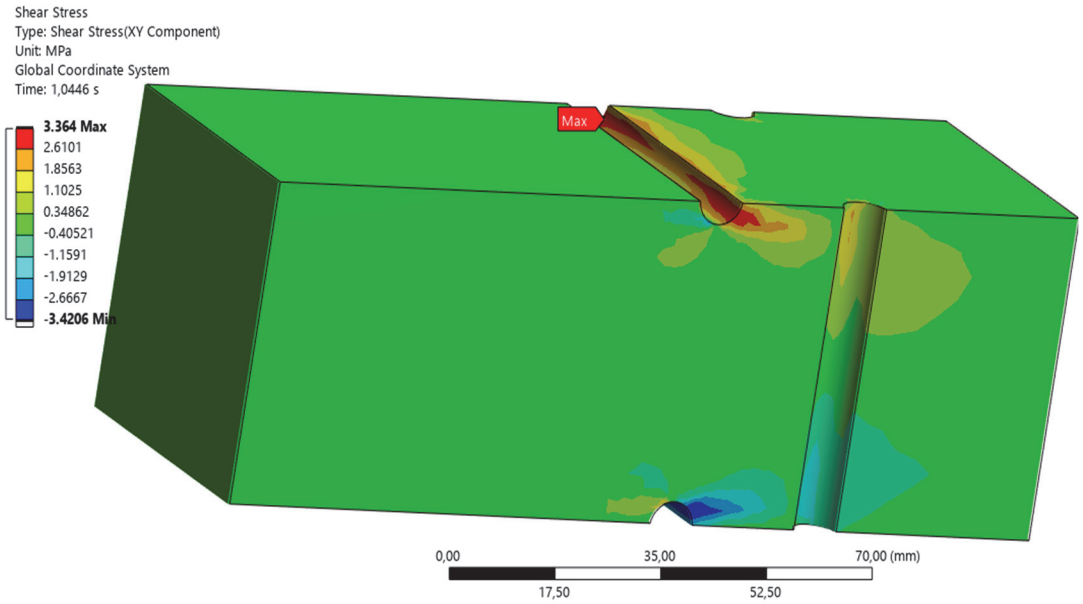

Figure 6: Visualization of results for limit milestones in the first loading scheme (axial tensile test): shear stress of timber variant No. 02.

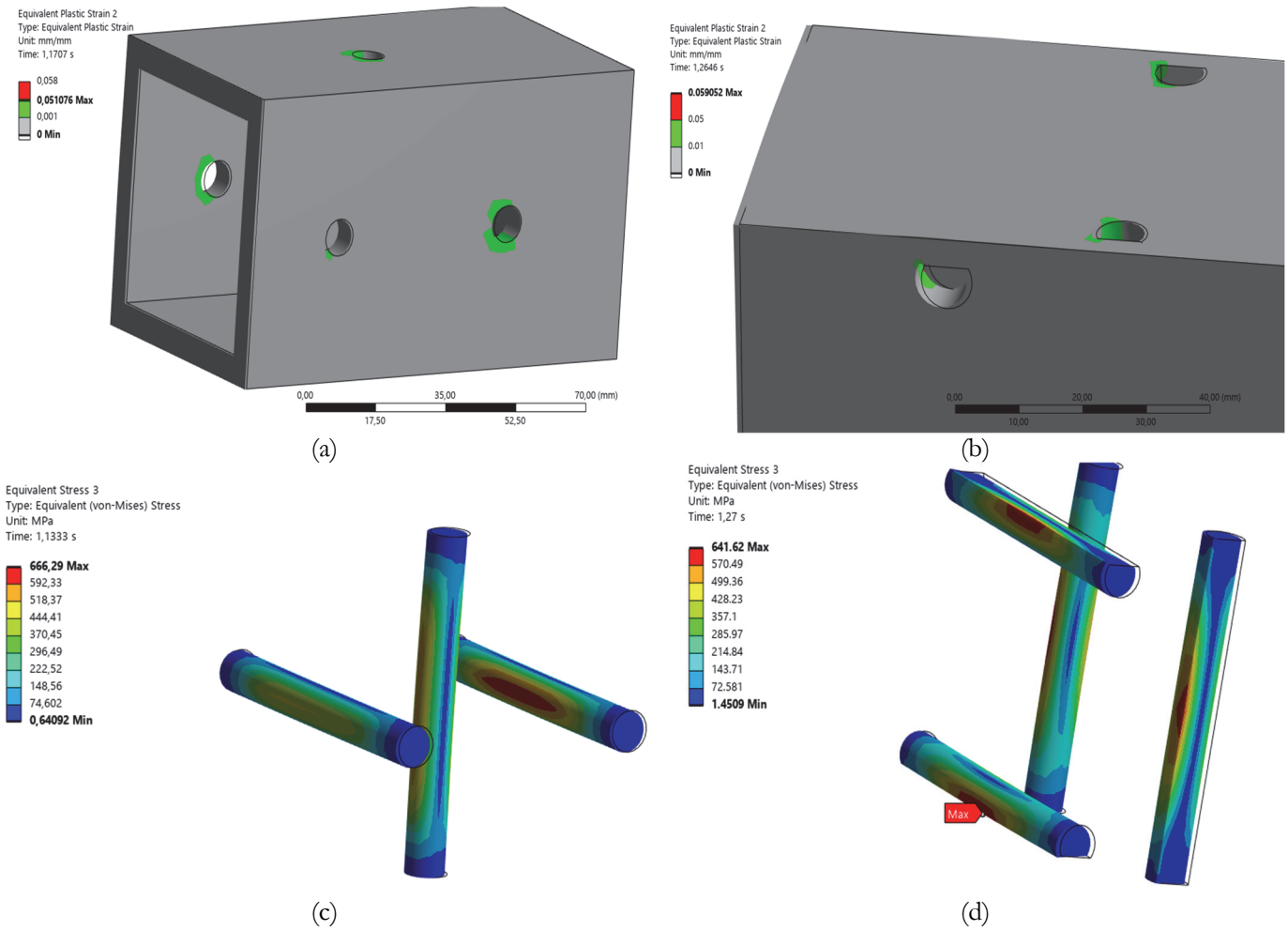

Figure 7: Visualization of results for limit milestones in the first loading scheme (axial tensile test): equivalent plastic strain of PC blend (a) variant No. 01, (b) variant No. 02; equivalent stress for steel (c) variant No. 01, (d) variant No. 02.

Second load scheme: three-point bending test in Z direction

The second set of results is again represented by a force-displacement diagram (see Fig. 8). These are the results from the three-point bending model with loading in the Z-axis direction. As mentioned above, the resulting force has been multiplied by two to match the real static diagram. This will make it possible to compare the results with the test in the future. Again, the limits for each material are shown. Geometric Variant 02 shows a different resistance distribution than Variant 01. The wooden part of variant 02 has small resistivity, but PC blend and steel have a higher performance. Figs. 9 to 11 shows the visualization of the individual limit values of the separate components (by material).

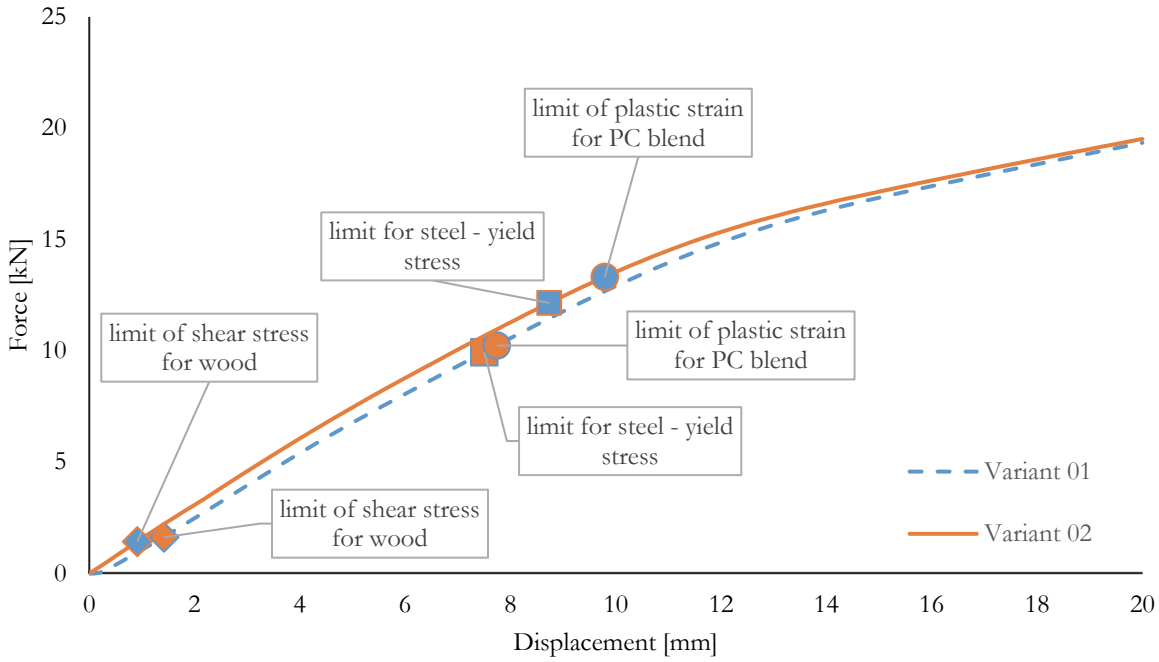

Figure 8: Force-displacement diagram for second load scheme (three-point bending test in Z direction) for variants 01 and 02 with critical points for each material.

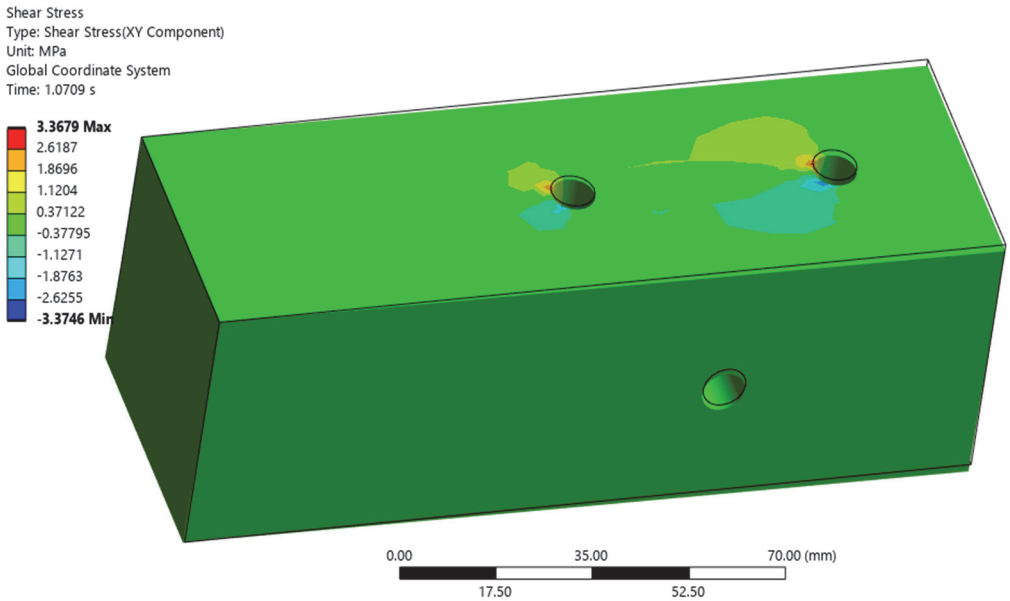

Figure 9: Visualization of results for limit milestones in second load scheme (three-point bending test in Z direction): shear stress of timber variant No. 01.

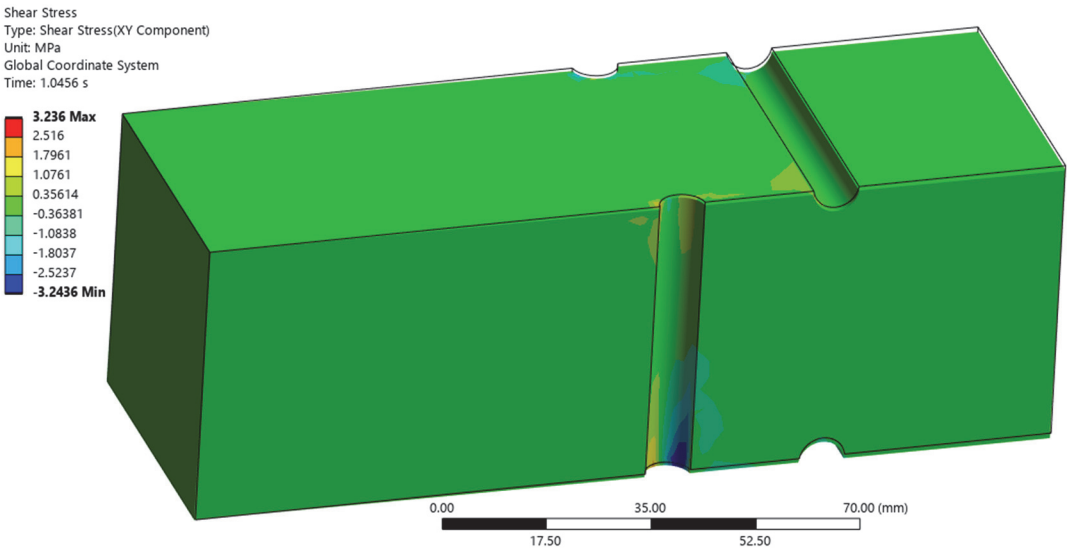

Figure 10: Visualization of results for limit milestones in second load scheme (three-point bending test in Z direction): shear stress of timber variant No. 02.

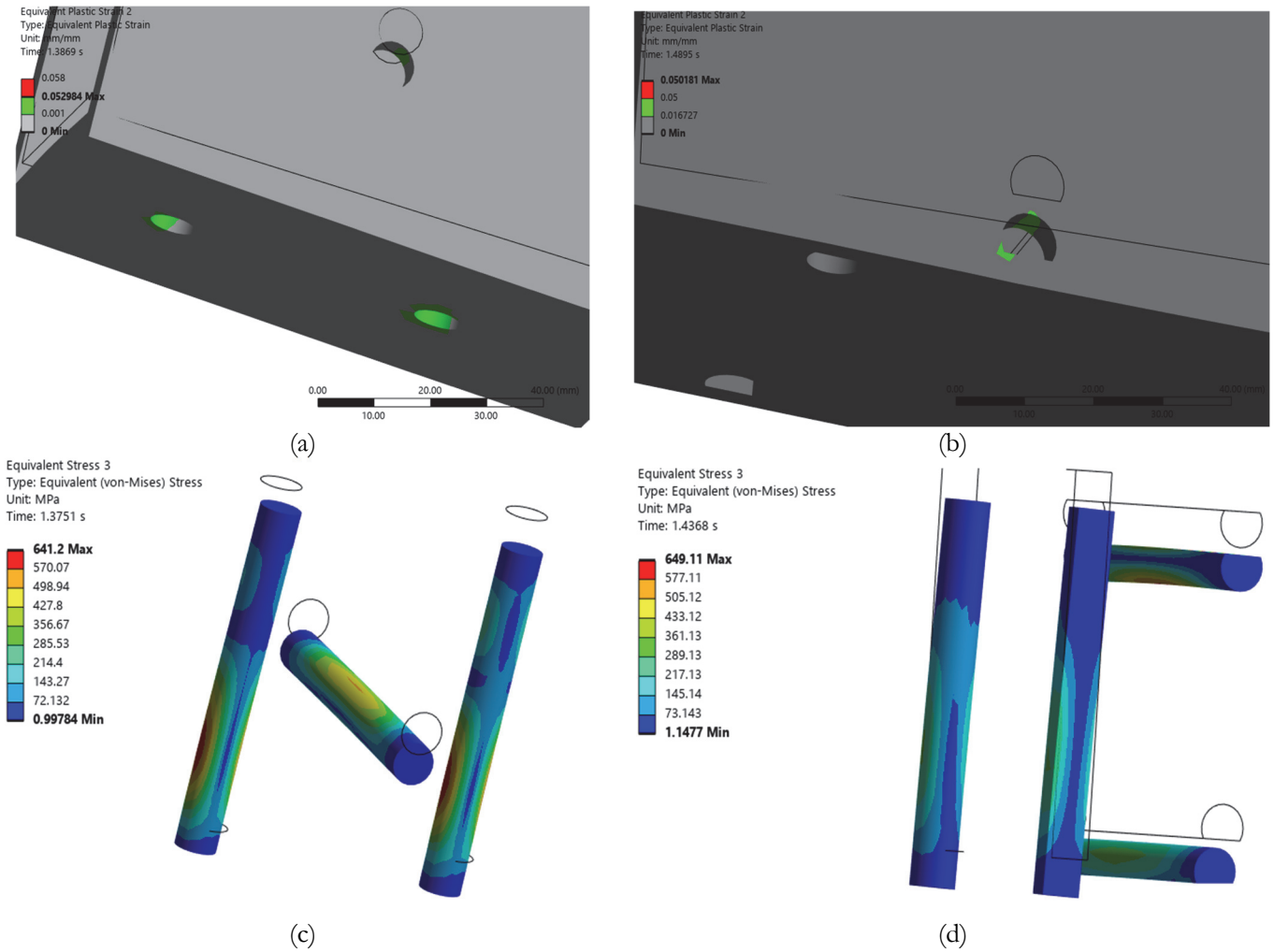

Figure 11: Visualization of results for limit milestones in second load scheme (three-point bending test in Z direction): equivalent plastic strain of PC blend (a) variant No. 01, (b) variant No. 02; equivalent stress for steel (c) variant No. 01, (d) variant No. 02.

Third load scheme: three-point bending test in Y direction

The third set of results is again represented by a force-displacement diagram (see Fig. 12). These are the results from the three-point bending model with loading in the Y-axis direction. As mentioned above, the resulting force was multiplied by two to match the actual static diagram. This will allow future comparison of the results with the test. Again, the limiting values for each material are given. Reversing the direction of loading did not significantly change the diagrams themselves but did shift the limit values in both directions for the different materials. Variant 02 again shows the highest limit for steel, but the PC blend does not produce better performances here than in variant 01. Figs. 13 to 15 shows a visualization of the individual component limits (by material).

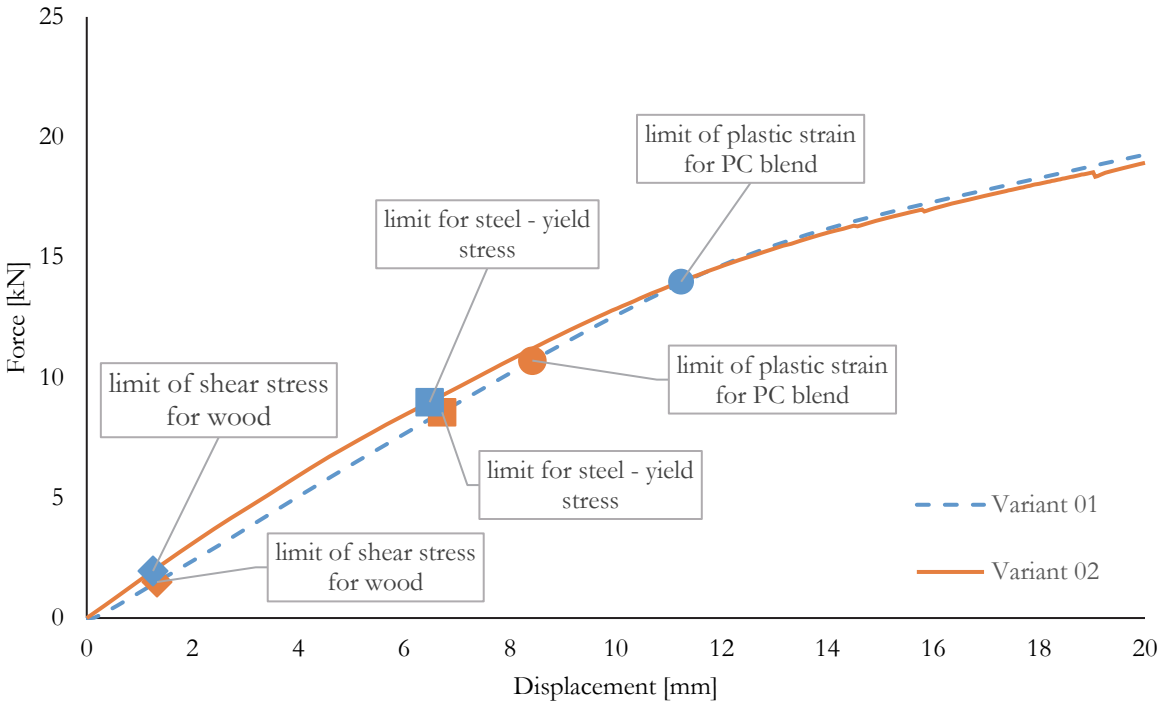

Figure 12: Force-displacement diagram for third load scheme (three-point bending test in Y direction) for variants 01 and 02 with critical points for each material.

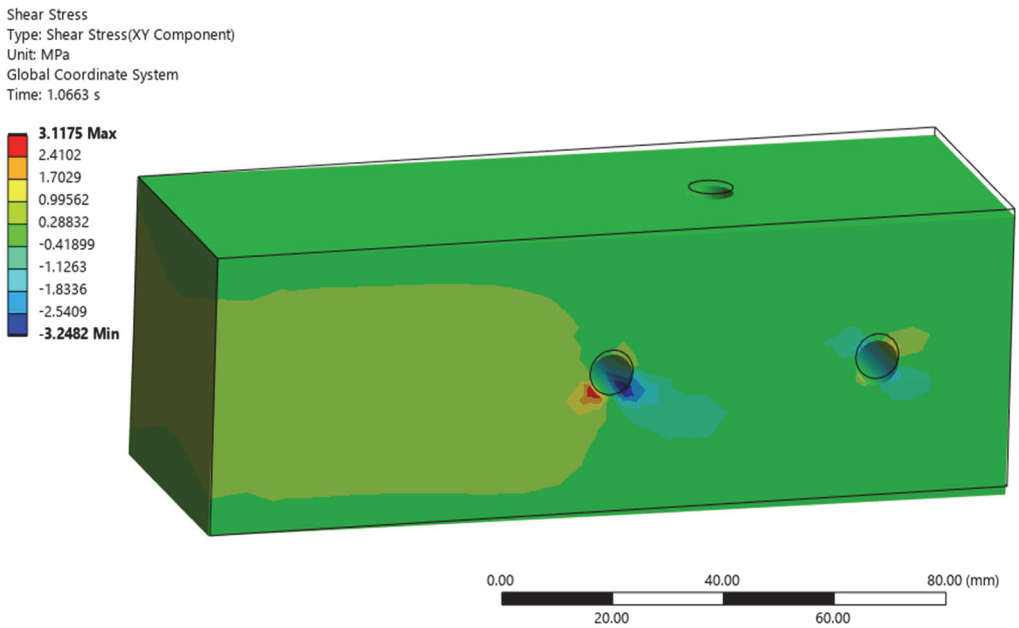

Figure 13: Visualization of results for limit milestones in the third load scheme (three-point bending test in Y direction): shear stress of timber variant No. 01.

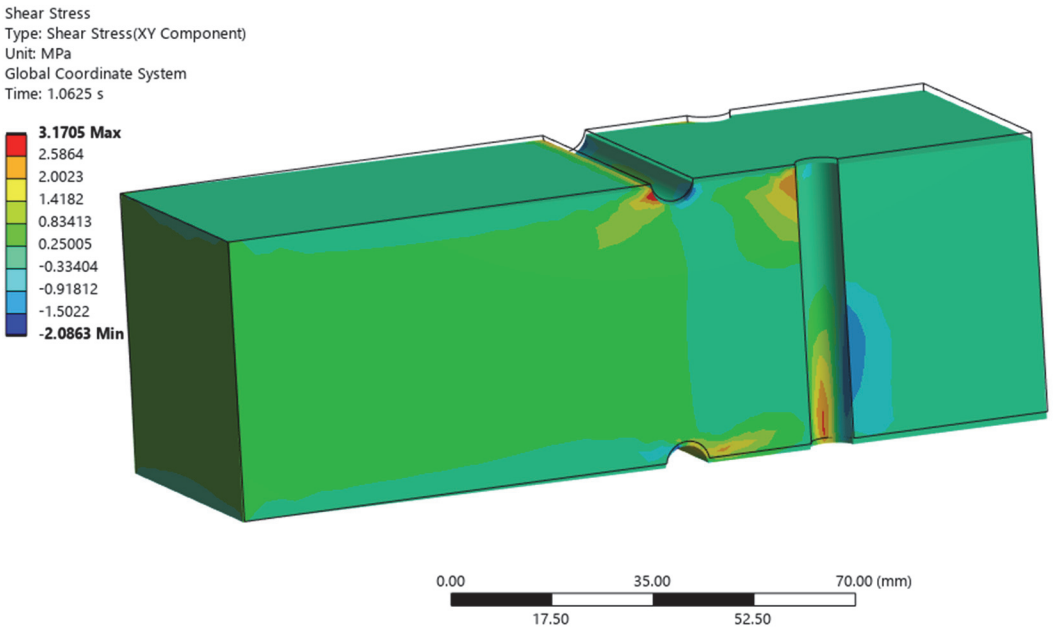

Figure 14: Visualization of results for limit milestones in the third load scheme (three-point bending test in Y direction): shear stress of timber variant No. 02.

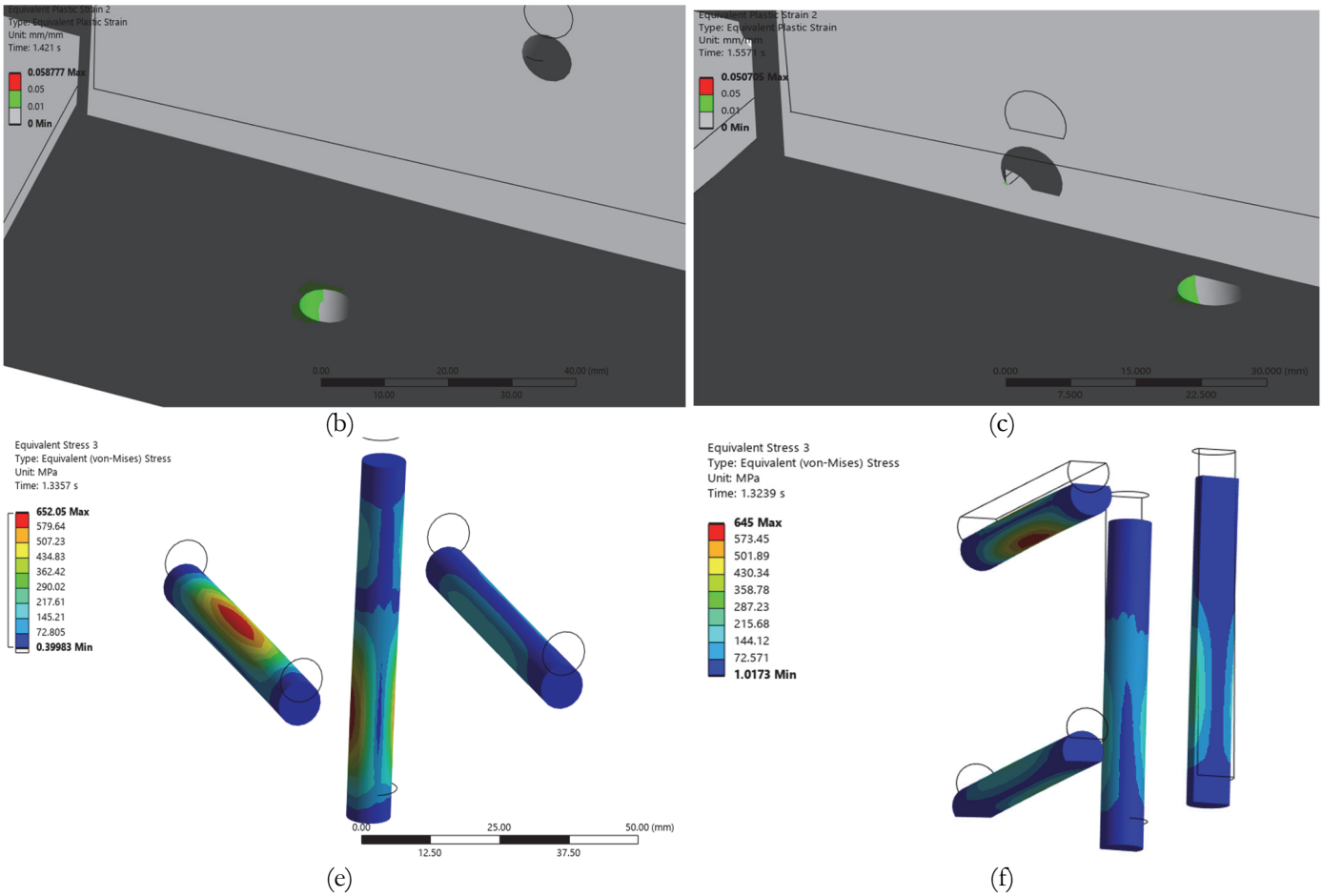

Figure 15: Visualization of results for limit milestones in the third load scheme (three-point bending test in Y direction): equivalent plastic strain of PC blend (a) variant No. 01, (b) variant No. 02; equivalent stress for steel (c) variant No. 01, (d) variant No. 02.

Fatigue analysis

The fourth set of results is represented by the number of load cycles in each element (node) of the 3D printed joint (see Fig. 16). This is a greatly simplified analysis. Comparison of the two geometrical variants is possible at the level of the ratio between maximal values. In this case, Variant 01 shows approximately three times more resistance to cyclic load-induced failure. The reason for this disproportion is probably the shape of the pins in variant 2, which is deliberately not a pure circle. The critical areas of Variant 01 are concentrated around the pin holes. In variant 02, there are also pin holes, but the critical area is in the voltage concentrator, in the change in hole geometry.

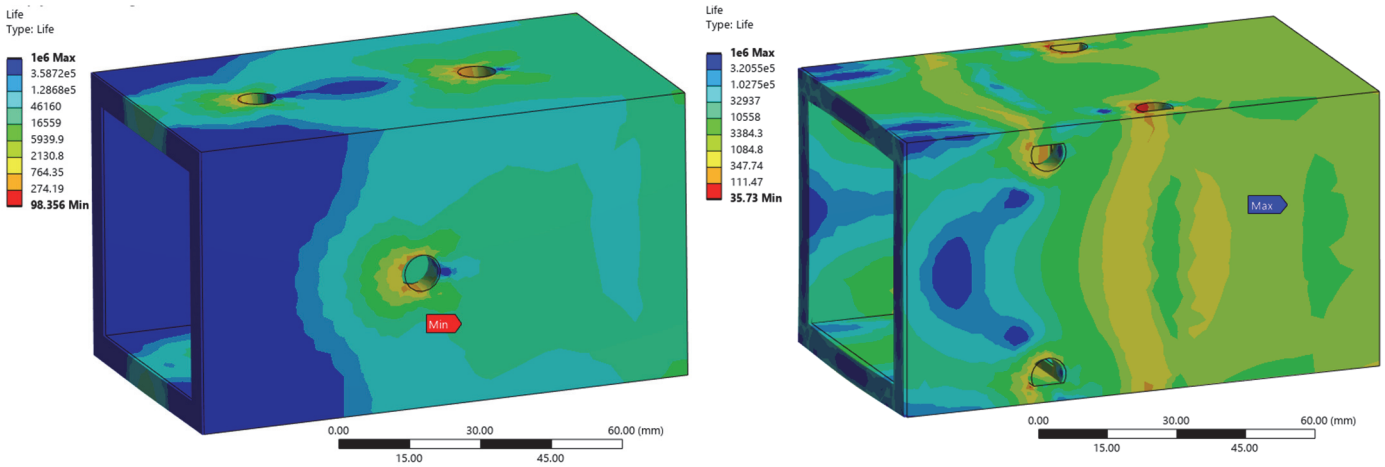

(a) (b)

Figure 16: Visualization of results of stress life cycle analysis: (a) geometric variant 01, (b) geometric variant 02.

SUMMARY

Two geometrical variants have been presented with different ways of connecting the 3D printed (from polycarbonate) element and the wooden element. These variants were modelled and loaded in four different loading schemes. The examples given here will serve as a basic design stage for real printed joints that will undergo experimental testing (see prototype of variant 01 in Fig. 17). This will make it possible to verify the models and then use them for more complex geometric variants. It should be stressed that the material properties were taken from the literature and previous research. Before the experimental phase, it will be necessary to prepare material analyses of the basic parameters so that the evaluation of the models is as accurate as possible.

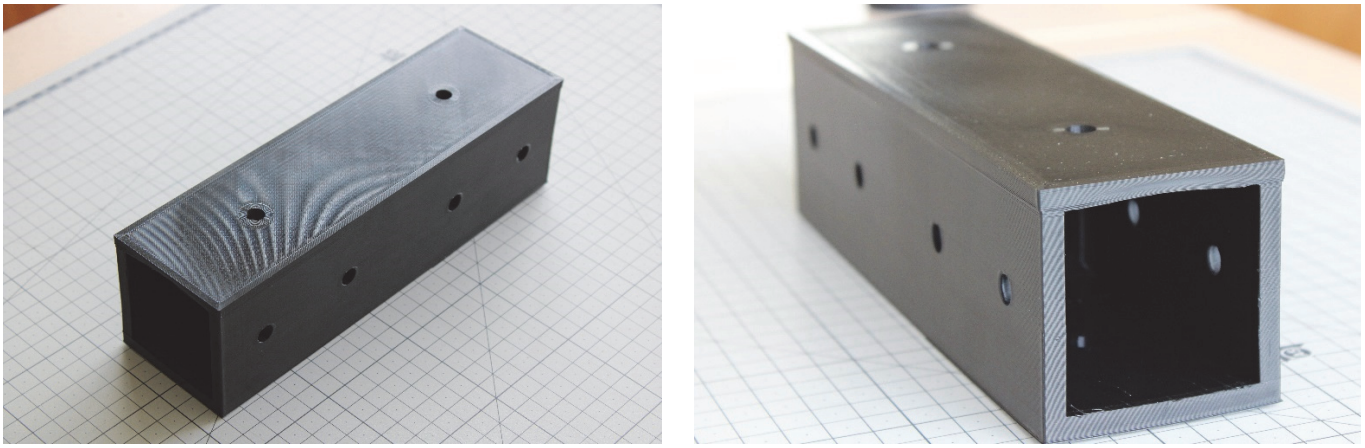

Figure 17: Photos of the prototype of variant 01 prepared for experimental testing.

The first three loading schemes were used for the analysis of the mechanical properties of the joints and the last one for the analysis of the simplified fatigue behavior. The first scheme was the axial tension test. The results showed a significantly higher performance for the 02 variant in the tensile test. Furthermore, different distributions were observed between the materials to the limit values. However, it should be considered that for variant 02 there is theoretically a larger contact area between the materials analyzed. This needs to be investigated in the future.
For loading schemes two and three, i.e. three-point bending in two perpendicular directions, similar test behaviour could be observed. However, the critical locations of the limit values are different. Variant 02 is prepared as more symmetrical (same number of pins in both axes), but the results from two different loading directions are different in terms of limit points. Also, in these cases in both schemes, Variant 02 came out better. The fourth loading scheme was prepared for simplified stress live cycling analysis. The results of the number of cycles for the two geometrical variants were directly compared. Variant 01 showed three times higher resistance than variant 02. This may be due to the shape of the pin holes, which is not a circle but a cut circle. Fatigue analysis needs the inclusion of real load history in the future or the application of other more complex calculations.

Conclusions

Combining traditional materials with new techniques and knowledge can lead to greater sustainability and reduced construction and renovation costs. An example is the application of 3D printing in the development or design of different parts of building structures. This paper presents the basic principles, prerequisites and procedures for the numerical analysis of 3D printed joints for timber structures using the finite software method. Results from several loading schemes on two geometries with significantly different wood and 3D printed material interactions have been presented. One scheme was designed for simplified fatigue analysis. The results from the schemes prepared for performance analysis of both variants showed that variant 02 has a higher resistance to static loading. On the other hand, in the case of fatigue evaluation, variant 01 is more suitable. It is clear that the advantages of one option do not outweigh the advantages of the other, so it is desirable to prepare a combined or new geometry. The presented procedure adopts some simplifications and involves several compromises. However, it has the advantage of a high level of effort to outline a comprehensive path suitable for comparing different geometric variations of 3D printed connections in timber frame structures. Future research will focus on verification through an experimental program, expanding the types of loading schemes and design variations to take full advantage of the benefits of 3D printing. Also, it can be interesting to evaluate the crack initiation and propagation in a 3D printed element or the fracture toughness of an element.

Acknowledgment

This research and this paper were funded by the Ministry of Education, Youth and Sports of the Czech Republic in Student Grant Competition through VSB – Technical University of Ostrava – grant number: SGS SP2024/093.

References

[1] American Society for Testing and Material (ASTM). (2006). ASTM D 143-94 Standard Test Methods for Small Clear Specimens of Timber (Reapproved 2000).
[2] American Society for Testing and Materials. (2016). ASTM D638-14, ASTM International, 82(C).
[3] ANSYS. (2020). ANSYS Meshing User's Guide. ANSYS User Guide. Available at: https://customercenter.ansys.com/.
[4] ASTM International. (2003). ASTM D790, Annual Book of ASTM Standard, i.
[5] Bakhtiari, H., Aamir, M., Tolouei-Rad, M. (2023). Effect of 3D Printing Parameters on the Fatigue Properties of Parts Manufactured by Fused Filament Fabrication: A Review, Applied Sciences (Switzerland). DOI: 10.3390/app13020904.
[6] Bathe, K.-J. (2008). Finite Element Method., Wiley Encyclopedia of Computer Science and Engineering, Hoboken, NJ, USA, John Wiley & Sons, Inc.
[7] Dedek, J., Juračka, D., Bujdoš, D., Lehner, P. (2024). Mechanical Properties of Wooden Elements with 3D Printed Reinforcement from Polymers and Carbon, Materials, 17(6). DOI: 10.3390/ma17061244.

[8] Ernur, A., Akiner, İ., Akiner, N., Zileska-Pancovska, V. (2022). Using wood as a new generation building material in the context of sustainable development, Zastita Materijala, 63(1), pp. 68–78. DOI: 10.5937/zasmat2201068A.
[9] Federowicz, K., Techman, M., Skibicki, S., Chougan, M., El-Khayatt, A.M., Saudi, H.A., Błyszko, J., Abd Elrahman, M., Chung, S.Y., Sikora, P. (2023). Development of 3D printed heavyweight concrete (3DPHWC) containing magnetite aggregate, Mater Des, 233. DOI: 10.1016/j.matdes.2023.112246.
[10] Ghanbari-Ghazijahani, T., Kasebahadi, M., Hassanli, R., Classen, M. (2022). 3D printed honeycomb cellular beams made of composite materials (plastic and timber), Constr Build Mater, 315. DOI: 10.1016/j.conbuildmat.2021.125541.
[11] Johanides, M., Lokaj, A., Dobes, P., Mikolasek, D. (2022). Numerical and Experimental Analysis of the Rotational Stiffness of a Timber Semi-Rigid Dowel-Type Connection, Materials, 15(16). DOI: 10.3390/ma15165622.
[12] Johanides, M., Lokaj, A., Dobes, P., Mikolasek, D. (2022). Numerical and Experimental Analysis of the Load-Carrying Capacity of a Timber Semi-Rigid Dowel-Type Connection, Materials, 15(20). DOI: 10.3390/ma15207222.
[13] Johanides, M., Mikolasek, D., Lokaj, A., Mynarcik, P., Marcalikova, Z., Sucharda, O. (2021). Rotational stiffness and carrying capacity of timber frame corners with dowel type connections, Materials, 14(23). DOI: 10.3390/ma14237429.
[14] Ketabdari, H., Saedi Daryan, A., Hassani, N. (2019). Predicting post-fire mechanical properties of grade 8.8 and 10.9 steel bolts, J Constr Steel Res, 162. DOI: 10.1016/j.jcsr.2019.105735.
[15] Khan, M.K.A., Alshahrani, H., Arun Prakash, V. (2023). Effect of grid pattern and infill ratio on mechanical, wear, fatigue and hydrophobic behaviour of abaca bracts biocarbon-ABS biocomposites tailored using 3D printing, Biomass Convers Biorefin. DOI: 10.1007/s13399-023-05196-4.
[16] Lüder, S., Härtel, S., Binotsch, C., Awiszus, B. (2014). Influence of the moisture content on flat-clinch connection of wood materials and aluminium, J Mater Process Technol, 214(10), pp. 2069–2074. DOI: 10.1016/J.JMATPROTEC.2014.01.010.
[17] Majid, F., Hachimi, T., Rhanim, H., Rhanim, R. (2022). Delamination effect on the mechanical behavior of 3D printed polymers, Frattura Ed Integrità Strutturale, 17(63), pp. 26–36. DOI: 10.3221/IGF-ESIS.63.03.
[18] Obara, P. (2018). Verification of Orthotropic Model of Wood, Archives of Civil Engineering, 64(3), pp. 31–44. DOI: 10.2478/ace-2018-0027.
[19] Ponikiewski, T., Katzer, J., Bugdol, M., Rudzki, M. (2015). X-ray computed tomography harnessed to determine 3D spacing of steel fibres in self compacting concrete (SCC) slabs, Constr Build Mater. DOI: 10.1016/j.conbuildmat.2014.10.024.
[20] Prusa i3. (2022). Original Prusa i3 MK3S+ 3D printer | Original Prusa 3D printers directly from Josef Prusa. PRUSA Research.
[21] Puigoriol-Forcada, J.M., Alsina, A., Salazar-Martín, A.G., Gomez-Gras, G., Pérez, M.A. (2018). Flexural fatigue properties of polycarbonate fused-deposition modelling specimens, Mater Des, 155. DOI: 10.1016/j.matdes.2018.06.018.
[22] Sánchez, M., Arrieta, S., Cicero, S. (2023). Fracture Load Estimations for U-Notched and V-Notched 3D Printed PLA and Graphene-Reinforced PLA plates using the ASED Criterion, Frattura Ed Integrità Strutturale, 17(66), pp. 322–338. DOI: 10.3221/IGF-ESIS.66.20.
[23] Su, A., Al'Aref, S.J. (2018). History of 3D Printing, 3D Printing Applications in Cardiovascular Medicine, pp. 1–10. DOI: 10.1016/B978-0-12-803917-5.00001-8.
[24] Tomei, V., Grande, E., Imbimbo, M. (2024). Optimization of the internal structure of 3D-printed components for architectural restoration, Frattura Ed Integrità Strutturale, 18(70), pp. 227–241. DOI: 10.3221/IGF-ESIS.70.13.
[25] Vassiliou, V., Barboutis, I., Kamperidou, V. (2016). Strength of corner and middle joints of upholstered furniture frames constructed with black locust and beech wood, Wood Research, 61(3).